Hindawi
Advances in Civil Engineering
Volume 2022, Article ID 2706897, 9 pages
https://doi.org/10.1155/2022/2706897

Research Article

Study on Backfill Acoustic Emission Characteristics and Source Location under Uniaxial Compressive

Caixing Shi,[1,2] Yicheng Wu,[3] Lijie Guo ,[1,2] Yue Zhao ,[1,2] and Wenyuan Xu[1,2]

[1]*BGRIMM Technology Group, Beijing 102628, China*
[2]*National Centre for International Research on Green Metal Mining, Beijing 102628, China*
[3]*Wu Shan Copper Mine of Jiangxi Copper Corporation, Ruichang 332204, China*

Correspondence should be addressed to Lijie Guo; guolijie@bgrimm.com

Received 10 January 2022; Accepted 1 February 2022; Published 21 February 2022

Academic Editor: Dawei Yin

This study investigates the acoustic emission (AE) characteristic of cemented tailings backfill (CTB) under uniaxial compressive loading. A classified tailings material source from Wushan Copper Mine was used to prepare cylindrical CTB samples. This study used an SLB10 loading machine for the uniaxial compressive test. A PCI-2 acoustic wave system was attached to the CTB specimen to measure the acoustic emission during loading. Overall, the backfill specimen's uniaxial compressive strength (UCS) is 3.58 MPa. The failure modes of the CTB sample could be divided into five stages, including the pore microfracture compacting stage (stage-a), linear elastic deformation stage (stage-b), yield deformation stage (stage-c), failure stage (stage-d), and residual stage (stage-e). At each stage, the AE characteristic parameters such as the hits per second (HPS), the cumulative number of impacts, energy rate, and total energy vary a lot, which indicates the AE parameter reflects the internal failure evolution of the CTB sample. In stage-a, no apparent AE behavior was measured. In Stage-b, there is no evident macroscopic change in the specimen, while the AE parameters steadily and continuously increase. During stage-c, the number of AE impacts grows sharply, the energy rate increases significantly, and changes suddenly. The cumulative number of AE impacts is 31.3% in stage-d, and the cumulative energy rate is 49.4%, which is the most active stage of acoustic emission activities. The specimen has prominent crack propagation and bifurcation phenomena. In stage-d, the CTB sample was destroyed entirely, and the characteristic parameters of acoustic emission were significantly reduced. Finally, multiple regression analysis methods are introduced into the time difference positioning method to locate the AE source. The positioning results show that the technique can better invert the close relationship between the damage and destruction of the CTB and the generation and penetration of the internal cracks and describe it to a certain extent. The failure surface of the filler specimen has an excellent guiding value for the analysis of the interior failure characteristics of the sample.

1. Introduction

The filling mining method has developed rapidly because of its characteristics of green environmental protection, high resource recovery rate, and practical ground pressure control [1–5]. Especially with the continuous extension of underground mining depth, the advantages of the filling mining method have become more pronounced [6–8]. The strength of cemented tailings backfill (CTB) is a key indicator of the filling mining technology since it is directly related to the safety of subsequent mining operations, and it is a source of worry for mining researchers [9–12]. Wen et al. [13] studied the factors that affect the strength of cemented backfill. The results show that the strength of cemented backfill is affected not only by single factors such as aggregate gradation, solid mass concentration, and cement content but also by the interaction of these factors. Mu et al. [14] studied the relationship between the strength of backfill and ultrasonic wave velocity and established a prediction model for the uniaxial compressive strength (UCS) of backfill based on the ultrasonic pulse velocity. Ercikdi et al. [15] show the linear relationship with a high correlation coefficient that appeared to exist between the UCS and ultrasonic pulse velocity UPV for CTB samples. Therefore, it is of great

significance to study the strength characteristics of the backfill and analyze the failure modes and failure laws at different stages to optimize backfill strength.

The CTB is a multiphase heterogeneous mixture with pores/cracks formed by mixing aggregate, cementing material, water, and solidifying after a certain curing age. It has complex mechanical properties. So it is necessary to study the damage and failure mode of backfill utilizing a new technology. At present, the scanning electron microscope (SEM) [16, 17], CT [18], UT (ultrasonic testing), and acoustic emission testing (AE) are used to study the internal failure mode of rock and soil specimens. When a material or structure is subjected to stress due to its microstructure's unevenness and defects, local stress concentration occurs, resulting in macroscopic manifestations such as plastic deformation, phase transformation, and cracking. In this process, a portion of the strain energy is released in a stress wave. This phenomenon of releasing strain energy in the form of an elastic stress wave is called acoustic emission (AE) [19], and the place where the wave occurs is called the acoustic emission source. AE testing technology uses sensors installed on the surface of materials to receive part of the stress waves transmitted to the surface to form a detection signal. Damage evaluation and research of materials can be realized through the detection, recording, and analysis of these signals [20, 21]. Cheng et al. [22] studied the influence of particle size on the mechanical properties of cemented backfill and obtained the strength of CTB and the characteristic parameters of AE. Sun et al. [23] studied the relationship between the AE signal and the failure of the backfill and constructed the constitutive damage model of the backfill. Zhao et al. [24] studied the relationship between AE event rate, ringing count rate, and stress-time through uniaxial compression and splitting failure tests. Cao et al. [25] investigated the compressive strength behavior and AE characteristics of 180-day cured CTB samples by using four different loading rates. The essential findings provided a scientific reference for studying the dynamic characteristics of CTB samples.

The results show that the AE parameters contain the damage information of the CTB and can describe the damage evolution process of the backfill. Still, the AE detection technique is not used to analyze the AE source.

Considering that wave velocity is also an important index for measuring rock mass failure [26], to comprehensively analyze the failure process of backfill mass, the mechanical properties of Wushan Copper Mine tailings are tested under uniaxial compression conditions. The AE technique analyzed the mechanical and AE characteristics of the backfill, and AE parameters characterized the failure mechanism of the backfill. On this basis, the method of time difference location is used to locate the AE source and verify the failure mechanism of the backfill.

2. Test Analysis

2.1. Basic Physical Properties of Tailings. The tailings used in the test were taken from the flotation workshop of the Wushan copper concentrator. Its density is 3.1 g/cm^3. Figure 1 shows the composition of grain size.

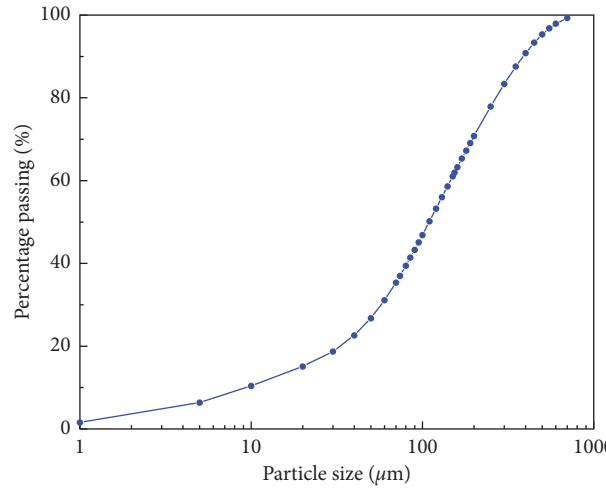

Figure 1: The particle size distribution of classified tailings.

The grain size distribution of the tailings determined as per relevant ASTM D422 is summarized in Figure 1. The grain size analysis shows the tailings contain 60% of the particles finer than 145.6 μm (d_{60}), 30% of the particles finer than 57.4 μm (d_{30}), and 10% of the particles are than 9.4 μm (d_{10}). The grain size analysis also shows it contains 37% of fine particles <74 μm and 22% of fine fractions <40 μm, which identifies the tailings as coarse sand. The calculated uneven coefficient, Cu is 15.54. As summarized in Figure 1, the grain size distribution curve slope is steep, and the curvature coefficient Cc is 2.4. The tailings particles are relatively uniform in size and are, however, poorly graded.

2.2. Sample Preparation. The cylindrical specimens were made according to the standard of ASTM D4832, and the dimensions were diameter × height: 55 mm × 110 mm. The specimen mass fraction is 74%, and the cement content is 20%. The prepared specimens were maintained in the YH-40B curing box with the curing parameters of 20°C, 95% humidity, and 28 days of age.

2.3. Sample Equipment and Method. The test instrument comprises an SLB100 press machine produced by Changchun Machinery and a PCI-2 AE system produced by PAC Company of the USA. Figure 2 shows the A.E. test system. The main shaft adopts displacement control in the experiment, and the loading rate is 0.003 mm/s. The PCI-2 AE system is connected to a computer, which can set, monitor, and store acoustic emission parameters and realize real-time control of AE signal collection. The AE probe contacts the specimen, and a preamplifier is connected between the probe and the acquisition card. The threshold value of the sensor signal acquisition is 45 dB.

In order to reduce the end restraint, two pieces of abrasive reducing paper are placed at both ends of the specimen, and a little butter is put between the two pieces of paper. Four AE probes are fixed on the surface of the CTB according to the space "cross" arrangement. Figure 3 shows the AE test method. The AE measurement point area is

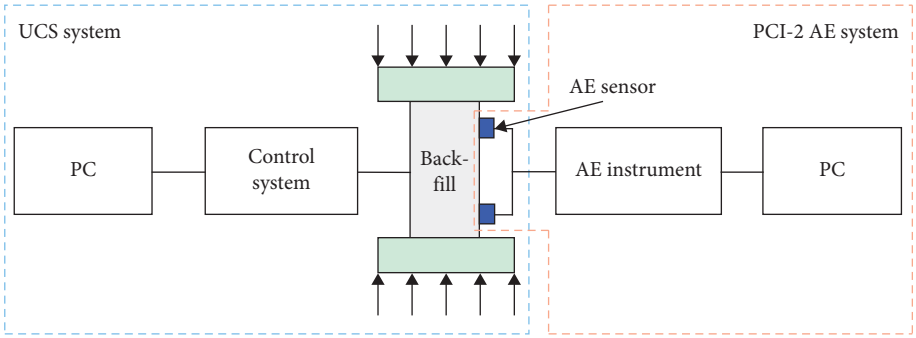

Figure 2: The logic diagram of the SLB100 loading machine and PCI-2 acoustic wave system.

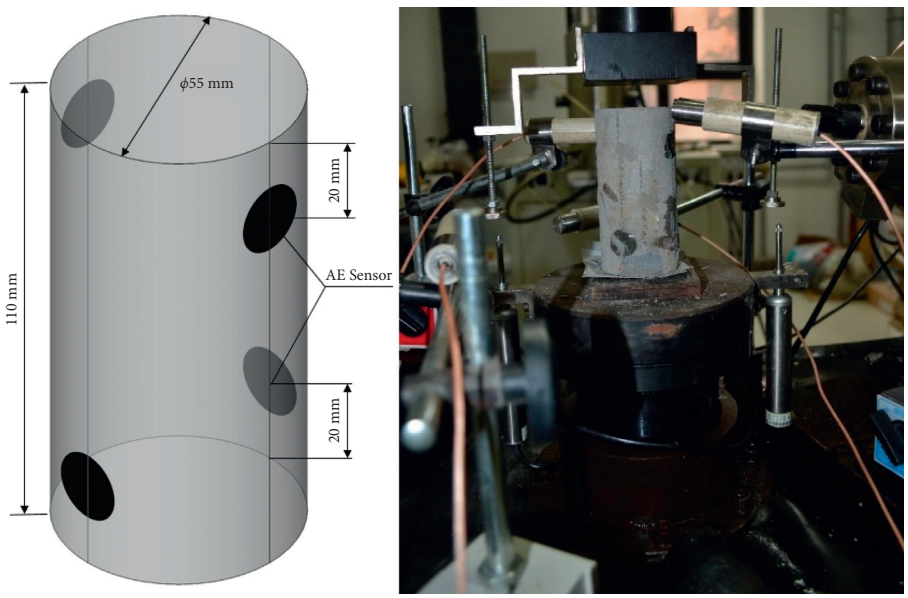

Figure 3: AE test method.

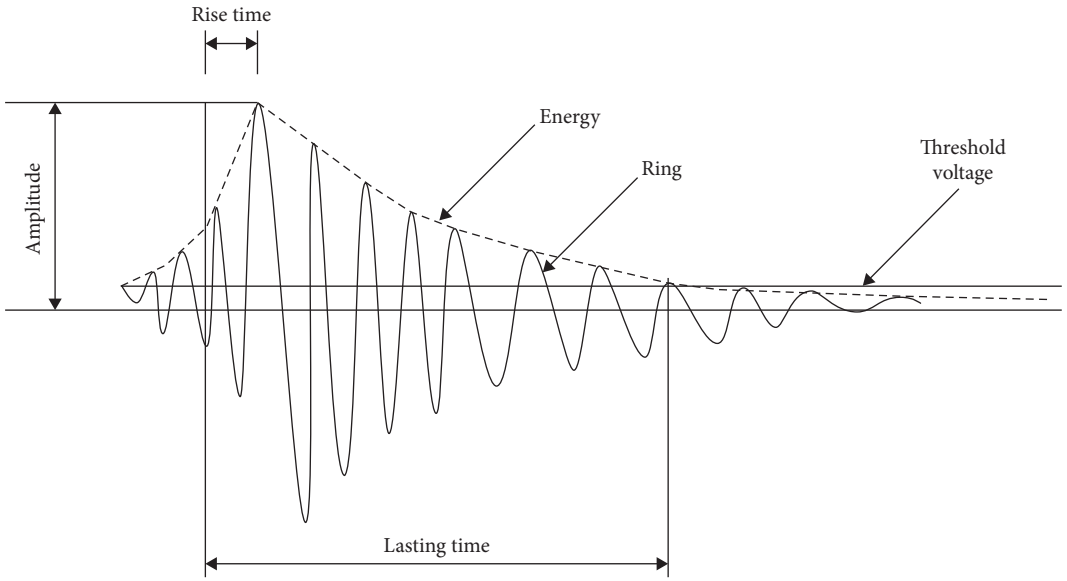

Figure 4: The diagram of acoustic emission characteristic parameters.

smoothed, and the smoothed area is 16 mm × 16 mm. After installing the radial displacement extensometer in the middle of the specimen, the SLB100 press completes the uniaxial loading. The control system and the AE detection system are used to collect the data in uniaxial compression until the loading is completed.

2.4. AE Characteristic Parameters. The CTB is an elasto-plastic material, and the stress wave will be released by the derivation and expansion of internal cracks during loading. The stress waves show different acoustic signals at different time intervals. An AE signal is a complex waveform containing a lot of information. Choosing the appropriate signal processing method to analyze acoustic emission signals is always a complex problem in developing AE detection technology. The characteristic parameter analysis is a standard method for AE signal analysis at present. The AE parameters commonly include impact (waveform) counting, ringing counting, energy, amplitude, lasting time, rise time, and threshold voltage. Figure 4 shows the specific meaning. The AE characteristic parameters are closely related to the signal of the same waveform; they appear or disappear simultaneously. Hence, they have similarities in describing the destruction mechanism of the specimen.

A hit is any signal that exceeds a threshold and causes a channel to acquire data. It reflects AE activities' total amount and frequency. The change in hit number demonstrates the transformation of the internal structure of the specimen. It can be used to characterize microcrack evolution [23, 27]. In this paper, the total number of AE hits per second (HPS) is adopted as the AE parameter for study. Energy is the area under the envelope of signal detection, reflecting the intensity of the signal, and is an important parameter indicating the material failure of the specimen, providing a basis for predicting the material instability failure.

3. AE Test Results and Analysis

In order to study the mechanical properties of backfill under uniaxial compression, the AE characteristic parameters such as HPS, cumulative HPS, energy rate, and energy were investigated. Considering that several groups of filling blocks' mechanical properties and AE characteristics are almost the same, only one group is selected as a type specimen for analysis.

According to the stress-time curve of the backfill under uniaxial compression in Figures 5–8, the UCS of the CTB is 3.58 MPa when the maximum compaction of the backfill is 8.5 KN. At the same time, the compression process of backfill can be divided into five stages, a–e: pore microfracture compacting stage (stage-a), linear elastic deformation stage (stage-b), yield deformation stage (stage-c), failure stage (stage-d), and residual stage (stage-e).

Stage-a: the stress-time curve of the backfill body is concave at the early stage of stress loading (0–53 s), and the number of hit times and energy rate in this stage are less. The cumulative HPS accounts for 2.4% of the total HPS number, and the energy accounts for 0.2% of the total energy. The results show that the AE activity is not active during stage-a, mainly because the CTB is artificially prepared and artificially stirred to ensure the excellent homogeneity and compactness of the filling body. There is less friction between the particles in the CTB during the compression process. There is no change in the appearance of the specimen.

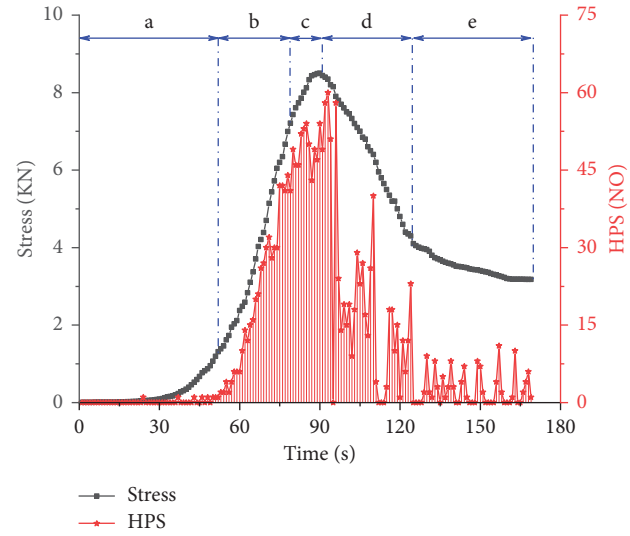

Figure 5: The stress-time curve and AE HPS-time curve of backfill under uniaxial compression.

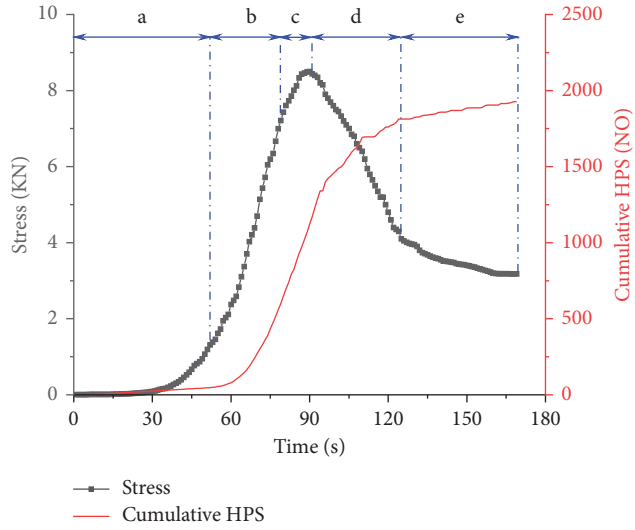

Figure 6: The stress-time curve and AE cumulative HPS-time curve of backfill under uniaxial compression.

Stage-b: with the increase of stress, in the 53 s–80 s period, the CTB enters the linear elastic stage, the loading curve is nearly straight, and the pressure is about 6.99 KN, reaching 82% of the maximum stress. At this stage, the pore/fractures in the backfill continue to compress, and microcracks begin to appear on the soft surface of the interior. The HPS and energy rate increase steadily. The cumulative HPS and energy rate account for 24.8% and 10.6%, respectively. From the

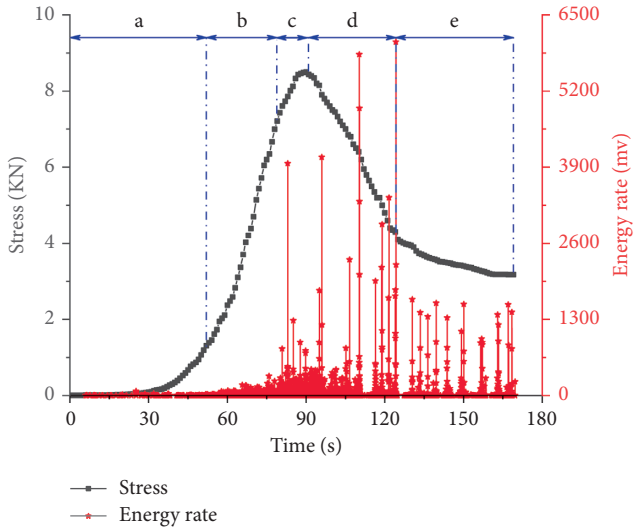

Figure 7: Stress-time curve and AE energy rate-time curve of backfill under uniaxial compression.

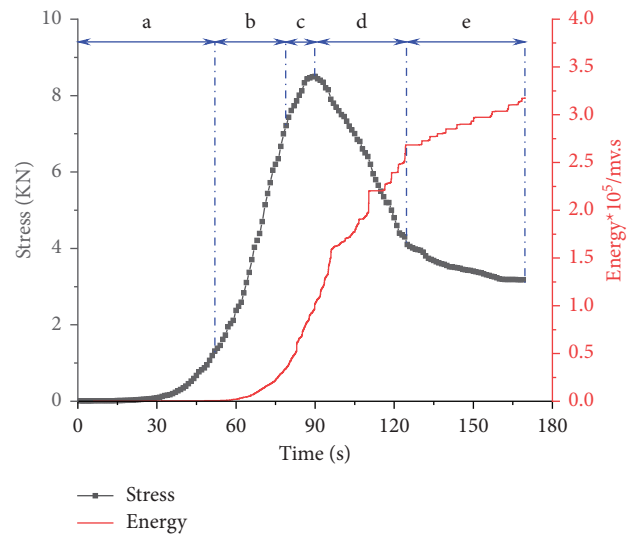

Figure 8: Stress-time curve and AE energy-time curve of under uniaxial compression.

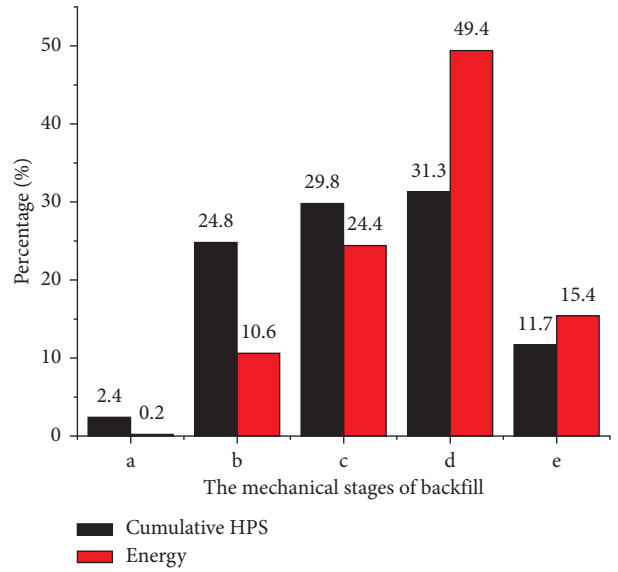

Figure 9: The proportion of A.E. signals in different stages.

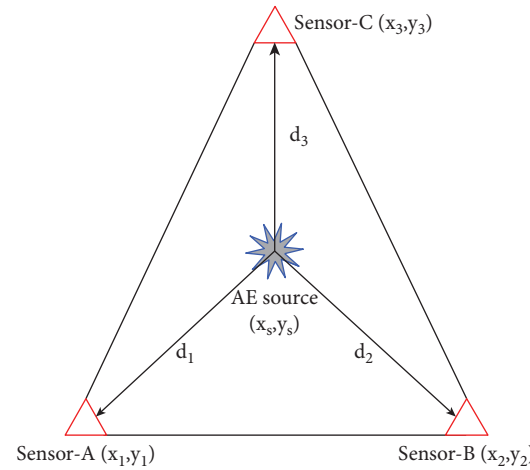

Figure 10: The schematic diagram of acoustic emission source positioning.

experimental process, there is no noticeable change in the macroscopic structure of the CTB, only a slight abscission at the end.

Stage-c: during the 80 s–91 s, the slope of the stress-time curve gradually decreases until it becomes zero, the loading stress reaches its peak value, the backfill enters the yield softening stage, and plastic deformation occurs. The microcracks will cause the stress adjustment of the stress frame after the grain bond fracture, which will lead to an increase in the stress near the grain and failure when the pressure near the grain reaches bond strength. The change in the stress transfer path and the weakening of the mechanical framework showed that the number of HPS increased sharply and approached the maximum value. The energy rate also increased obviously. There were two significant, abrupt changes, and the AE activity was active, indicating that pores/fractures in the CTB were accelerated. The accumulative HPS accounted for 29.8% of the total hits, and the accumulative energy rate accounted for 24.4% of the total energy. From the perspective of the test process, at this stage, the filling body began to show cracks on a macro scale, and the cracks continued to expand, gradually showing a certain penetration tendency.

Stage-d: during the period of 91 s to 125 s, after the loading stress reaches its peak value, the backfill body decays sharply, the pressure drops significantly, and the slope of the stress-time curve becomes negative. The number of HPS has been significantly reduced but is still relatively strong. It is mainly due to the continuous accumulation of internal damage as the cracks in the CTB expand and increase, finally

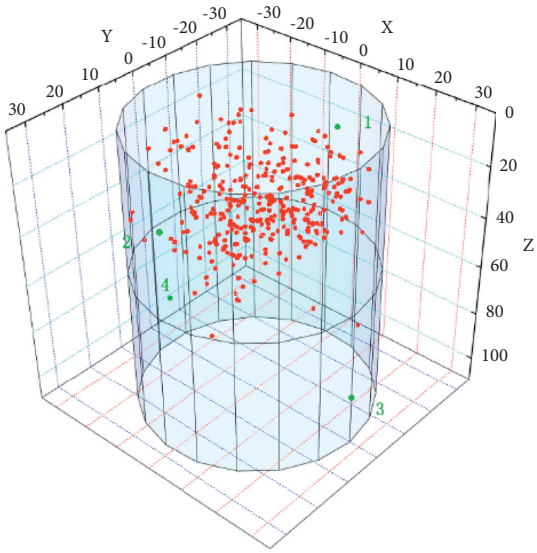

Figure 11: The result diagram of acoustic emission source location result diagram.

Figure 12: The final destruction diagram of the filling body.

forming a macroscopic fracture surface that affects the propagation of elastic waves inside the filling body, resulting in the AE signal being reduced. But the rupture of the backfill will produce many elastic waves, which will make the energy rate abrupt many times and reach the highest value. From the test process, the appearance of the CTB has apparent crack growth and bifurcation phenomena, and the small cracks gradually penetrate the large cracks, causing apparent damage.

Stage-e: during the 125 s to 170 s, the speed of stress reduction is slowed down. Because the filling body still has a specific bearing capacity, the stress is maintained at a lower level and does not decrease to zero. At this stage, the AE HPS in the backfill reduces significantly, and the accumulative hits increase slowly, almost no more. The AE energy rate is a small peak of abrupt change, mainly caused by the sound produced by the partial breakage and shedding of the filling body. In this stage, the accumulative HPS accounts for 11.7% of the total hits, and the accumulative energy rate accounts for 15.4% of the total energy. The filling specimen mainly shows the block sliding along the macroscopic fracture surface from the test process until failure.

Based on the above analysis, there are five mechanical stages in the failure process of backfill under uniaxial compression, and each stage has a different form. The AE signal also shows prominent stage characteristics, indicating that the AE characteristic parameters can reflect the CTB's internal failure evolution law.

Figure 9 shows the cumulative HPS and energy rate in different mechanical stages. In stage-d, the cumulative HPS is 31.3%, and the cumulative energy rate is 49.4%, all of which reach the maximum value. There are apparent crack propagation and bifurcation in the filling body. And many new cracks are produced simultaneously, which is the most active stage of AE activity. Therefore, it is verified that the characteristic emission parameters can characterize the evolution law of primary crack propagation and penetration in the filling body.

4. Exploration and Analysis of AE Source Location

4.1. Calculation Method for AE Source Location. AE source location is an essential work in the AE test, and it is also an important index in AE detection and evaluation. The main methods of location are time difference location and area location [28–30]. The time difference location is based on the time difference between the AE signals from the same AE source arriving at different sensors, combining the parameters such as wave velocity and the distance between sensors. [31]. Figure 10 shows the principle of source positioning in a two-dimensional plane. This paper studies the AE localization of the CTB under uniaxial compression using the time difference localization method.

For an AE hit, the absolute time of transmission to the sensor is t. The distance d between the sensor and the sound source can be calculated by combining the sound velocity v.

$$d = v * t. \tag{1}$$

According to Pythagorean's theory, the distances between two points in a plane are

$$\mathrm{d} = \sqrt{(x_2 - x_1)^2 + (y_2 - y_1)^2}. \tag{2}$$

Since the absolute time of an AE event cannot be obtained, in this paper, we calculate the absolute distance between different sensors and AE sources. That is

$$t_{\mathrm{i}} - t_1 = \frac{(d_i - d_1)}{v}. \tag{3}$$

From the available data from formulas (2) and (3), we get

$$t_i - t_1 = \frac{\left[\sqrt{(x_i - x_s)^2 + (y_i - y_s)^2} - \sqrt{(x_1 - x_s)^2 + (y_1 - y_s)^2}\right]}{v}. \tag{4}$$

In the equation, X_S and Y_S are the AE sources coordinate.

The location of the sound source can be obtained by obtaining multiple sensor data using formula (4) simultaneously. The mathematical method becomes more complicated when it extends to 3D or rolls up the envelope into a 3D object, but the basic principle remains the same.

The standard methods of time difference location are the least square method, Geiger linear location method, multievent location method, etc. [32]. This paper introduces multiple regression analysis to search for the most suitable location among all source location data.

Suppose the observed time difference between the two sensors receiving the hit signal is

$$\Delta t_{i,\mathrm{obs}} = t_i - t_1. \tag{5}$$

The calculated time difference between the two sensors that receive the impact signal is defined as follows:

$$\Delta \mathrm{t}_{i,\mathrm{cal}} = \frac{\left[\sqrt{(x_i - x_s)^2 + (y_i - y_s)^2 + (z_i - z_s)^2} - \sqrt{(x_1 - x_s)^2 + (y_1 - y_s)^2 + (z_1 - z_s)^2}\right]}{v}. \tag{6}$$

Multiple regression analysis is a general-purpose global objective algorithm that minimizes the difference between $\Delta t_{i,\mathrm{obs}}$ and $\Delta t_{i,c1c}$. Therefore, we define the sum of the squares of the difference $\Delta t_{i,\mathrm{obs}}$ and $\Delta t_{i,c1c}$ as χ^2. That is

$$\chi^2 = \sum\left(\Delta t_{i,\mathrm{obs}} - \Delta t_{i,\mathrm{cal}}\right)^2. \tag{7}$$

The χ^2 is called the fitness value, which depends on the coordinated value corresponding to the source location, and the calculation process is an iterative searching process. This article uses the simplex search method to write the locator code to find the minimum value of x_s, y_s, and z_s.

4.2. Results and Analysis of AE Source Location. In order to study the internal failure characteristics of the filling material, the experiment was based on the improved time difference location method to conduct AE localization analysis. Before carrying out the AE test, the average velocity of the sound wave in the CTB was measured at 1147.9 m/s. This indicates that the velocity of wave propagation in the CTB is very fast, and the time from one end to the other end is only 95.8 μs. Therefore, on the basis of fixed acoustic velocity, the AE test is carried out, and the location of the AE source is analyzed. The analysis results are shown in Figure 11. It can be seen that the AE source points are concentrated on the top of the specimen, and the cracks are interspersed and penetrated complicatedly. Through the analysis of internal and external location points, it is deduced that the failure mode of the specimen is mainly splitting failure, which is in good agreement with the actual collapse. It is shown that the improved method can be used to inverse the close relationship between the damage failure of the CTB and the generation and transfixion of internal cracks.

Compared with Figures 11 and 12, some edge cracks of the backfill specimen are not reflected in the process of sound source localization. There are two main reasons for the analysis. First, because of the anisotropy of the backfill material, the acoustic signal will scatter and attenuate in the process of propagation, especially after cracks occur in the specimen. It limits the propagation of AE signals in the CTB.

5. Conclusions

The density of tailings used in the experiment is 3.1 g/cm^3, and their particle size belongs to a discontinuous gradation. Based on the uniaxial compression test of CTB, the mechanical properties and AE characteristics of the whole compression process are analyzed. The main conclusions are as follows:

(1) The UCS of the CTB is 3.58 MPa when the mass fraction is 74%, the cement content is 20%, and the curing age is 28 days. The whole compression process of the backfill can be divided into five stages: the pore microfracture compacting stage, linear elastic deformation stage, yield deformation stage, failure stage, and residual stage.

(2) In the failure stage, the cumulative HPS is 31.3%, and the cumulative energy rate is 49.4%, all of which reach the maximum value. The filling body has apparent crack propagation, bifurcation, and many new cracks, which are the most active stages of AE activity.

(3) The multiple regression analysis methods are introduced in the time difference location method. The positioning results are concentrated on the top of the specimen, and the cracks are interspersed and penetrated complex, which is more consistent with the actual situation. However, some cracks are not reflected in the positioning results, mainly due to the anisotropic characteristics of the CTB material and the iterative calculation with a fixed sound wave velocity.

(4) The AE characteristic parameters can reveal the evolution of the original cracks in the CTB, which indicates that the AE technique is of great value in the analysis of the failure characteristics of the CTB.

Data Availability

The data used to support the findings of this study are available from the corresponding author upon request.

Conflicts of Interest

The authors declare that there are no conflicts of interest regarding the publication of this paper.

Acknowledgments

The authors would like to acknowledge the financial support from the National Key R&D plan Intergovernmental International Scientific and Technological Innovation Cooperation (Grant no. 2021YFE0102900), the Exploration fund of BGRIMM (no. 02-2127).

References

[1] A. Ghirian and M Fall, "Coupled thermo-hydro-mechanical-chemical behaviour of cemented paste backfill in column experiments. Part I: Physical, hydraulic and thermal processes and characteristics," *Engineering Geology*, vol. 164, pp. 195–207, 2013.

[2] A. X. Wu, Y Yang, H. Y. Cheng, and S. M. Chen, "Status and prospects of paste technology in China," *Chinese Journal of Engineering*, vol. 40, no. 5, pp. 517–525, 2018.

[3] Q.-L Zhang, Y.-T. Li, Q.-S. Chen, Y.-K. Liu, Y. Feng, and D.-L. Wang, "Effects of temperatures and pH values on rheological properties of cemented paste backfill," *Journal of Central South University*, vol. 28, no. 6, pp. 1707–1723, 2021.

[4] C. Q Chen, Y. B. Tao, Q. L. Zhang, and C. C. Qi, "The rheological, mechanical and heavy metal leaching properties of cemented paste backfill under the influence of anionic polyacrylamide," *Chemosphere*, vol. 286, Article ID 131630, 2022.

[5] C. X. Shi, L. J. Guo, and X. Z. Chen, "Experimental Study on the Law of flow and segregation of filing slurry in stope," *Gold Science and Technology*, vol. 26, no. 4, pp. 520–527, 2018.

[6] A. Wu, Z. Ruan, R. Bürger, S. Yin, J. Wang, and Y. Wang, "Optimization of flocculation and settling parameters of tailings slurry by response surface methodology," *Minerals Engineering*, vol. 156, Article ID 106488, 2020.

[7] D. S. Gu, "The development tendency of mining science and technology of underground metal mine," *Gold*, vol. 25, no. 1, pp. 18–22, 2004.

[8] W. G. Xiao, *Study on Filling Technology in Deep Mine*, Ph.D, Central South University, Changsha City,China, 2003.

[9] M. Fall, T. Belem, S. Samb, and M. Benzaazoua, "Experimental characterization of the stress-strain behaviour of cemented paste backfill in compression," *Journal of Materials Science*, vol. 42, no. 11, pp. 3914–3922, 2007.

[10] E. Yilmaz, T. Belem, and M. Benzaazoua, "Effects of curing and stress conditions on hydromechanical, geotechnical and geochemical properties of cemented paste backfill," *Engineering Geology*, vol. 168, pp. 23–37, 2014.

[11] Q. S. Chen, K. Luo, Y. M. Wang, X. Li, Q. Zhang, and Y Liu, "In-situ stabilization/solidification of lead/zinc mine tailings by cemented paste backfill modified with low-carbon bentonite alternative," *Journal of Materials Research and Technology*, vol. 17, 2022.

[12] P. Zhang, Q. Gao, Z. J. Wen, and T. Zhang, "Influencing factors on backfill strength and a combined strength prediction model," *Journal of Northeastern University*, vol. 42, no. 02, pp. 232–241, 2021.

[13] Z. J. Wen, B. Xiao, Q. Gao, and S. Yin, "Study on strength influencing factors and strength model of cemented backfill with mixed aggregate," *Arabian Journal of Geosciences*, vol. 14, no. 9, pp. 1–11, 2021.

[14] G. C. Mu, F. Deng, and Z. H. Lai, "Study on the relationship between strength and ultrasound velocity of cemented fill mass," *Industrial Minerals & Processing*, vol. 49, no. 10, pp. 1–3 + 53, 2020.

[15] B. Ercikdi, T. Yılmaz, and G. Külekci, "Strength and ultrasonic properties of cemented paste backfill," *Ultrasonics*, vol. 54, no. 1, pp. 195–204, 2014.

[16] C. E. Krohn and A. H. Thompson, "Fractal sandstone pores: automated measurements using scanning-electron-microscope images," *Physical Review B*, vol. 33, no. 9, pp. 6366–6374, 1986.

[17] A Timur, W. B. Hempkins, and R. M. Weinbrandt, "Scanning electron microscope study of pore systems in rocks," *Journal of Geophysical Research*, vol. 76, no. 20, pp. 4932–4948, 1971.

[18] R. A. Johns, J. S. Steude, L. M. Castanier, and P. V. Roberts, "Nondestructive measurements of fracture aperture in crystalline rock cores using X ray computed tomography," *Journal of Geophysical Research: Solid Earth*, vol. 98, pp. 1889–1900, 1993.

[19] D. Drozdenko, J. Bohlen, S. Yi, P. Minárik, F. Chmelík, and P. Dobroň, "Investigating a twinning-detwinning process in wrought Mg alloys by the acoustic emission technique," *Acta Materialia*, vol. 110, pp. 103–113, 2016.

[20] Z. Moradian, H. H. Ballivy, and B. Gerard, "Detection of cracking levels in brittle rocks by parametric analysis of the acoustic emission signals," *Rock Mechanics and Rock Engineering*, vol. 49, no. 3, pp. 785–800, 2016.

[21] Z.-Z. Zhang, F. Gao, and X.-J. Shang, "Rock burst proneness prediction by acoustic emission test during rock deformation," *Journal of Central South University*, vol. 21, no. 1, pp. 373–380, 2014.

[22] A. P. Cheng, F. S. Dong, P. F. Shu, and Z. X. Fu, "Mechanical properties and acoustic emission characteristics of continuous graded cemented backfill," *Journal of Huazhong University of Science and Technology (Nature Science Edition)*, vol. 49, no. 08, pp. 46–52, 2021.

[23] G. H. Sun, S. S. Wei, and X. X. Liu, "On the damage evolution of fillings based on acoustic emission characteristics," *Journal of Experimental Mechanics*, vol. 32, no. 01, pp. 137–144, 2017.

[24] K. Zhao, X. Yu, S. T. Zhu, Y. Zhou, Q. Wang, and J. Wang, "Acoustic emission investigation of cemented paste backfill prepared with tantalum–niobium tailings," *Construction and Building Materials*, vol. 237117523 pages, 2020.

[25] S. Cao, E. Yilmaz, W. Song, E. Yilmaz, and G. Xue, "Loading rate effect on uniaxial compressive strength behavior and acoustic emission properties of cemented tailings backfill," *Construction and Building Materials*, vol. 213, pp. 313–324, 2019.

[26] S. G. Wang, Y. R. Liu, X. Chen, and Q. Yang, "Failure analysis of pre-cracked specimen based on acoustic emission technique," *Journal of Hydroelectric Engineering*, vol. 38, no. 7, pp. 110–120, 2019.

[27] A. Y. Cao, G. C. Jing, L. M. Dou et al., "Damage evolution law based on acoustic emission of sandy mudstone under different uniaxial loading rate," *Journal of Mining & Safety Engineering*, vol. 32, no. 6, pp. 923–928 + 935, 2015.

[28] L. Geiger, *Probability Method for the Determination of Earthquake Epicenters from the Arrival Time Only*, pp. 60–71, Bulletin of Saint Louis University, Missouri, USA, 1912.

[29] J. A. Nelder and R. Mead, "A simplex method for function minimization," *The Computer Journal*, vol. 7, no. 4, pp. 308–313, 1965.

[30] M. S. Sambridge and B. L. N. Kennett, "A novel method of hypocentre location," *Geophysical Journal International*, vol. 87, no. 2, pp. 679–697, 1986.

[31] A. Tobias, "Acoustic-emission source location in two dimensions by an array of three sensors," *Non-destructive testing*, vol. 9, no. 1, pp. 9–12, 1976.

[32] C. Fu, *Research on Source Location Methods of Acoustic Emission Based on Material of Rock*, Ph.D. thesis, Northeastern University, Shenyang City,China, 2015.